

# Aromatic Methoxylation and Hydroxylation by Organometallic High-Valent Nickel Complexes

Wen Zhou,<sup>†</sup> Jason W. Schultz,<sup>†</sup> Nigam P. Rath,<sup>‡</sup> and Liviu M. Mirica<sup>\*,†</sup>

<sup>†</sup>Department of Chemistry, Washington University, One Brookings Drive, St. Louis, Missouri 63130-4899, United States

<sup>‡</sup>Department of Chemistry and Biochemistry, University of Missouri-St. Louis, One University Boulevard, St. Louis, Missouri 63121-4400, United States

**S** Supporting Information

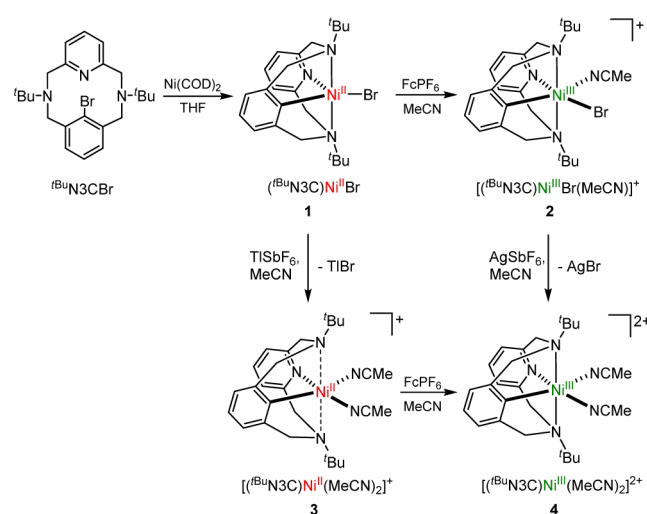
**ABSTRACT:** Herein we report the synthesis and reactivity of several organometallic Ni<sup>III</sup> complexes stabilized by a modified tetradentate pyridinophane ligand containing one phenyl group. A room temperature stable dicationic Ni<sup>III</sup>–disolvento complex was also isolated, and the presence of two available *cis* coordination sites in this complex offers an opportunity to probe the C–heteroatom bond formation reactivity of high-valent Ni centers. Interestingly, the Ni<sup>III</sup>–dihydroxide and Ni<sup>III</sup>–dimethoxide species can be synthesized, and they undergo aryl methoxylation and hydroxylation that is favored by addition of oxidant, which also limits the  $\beta$ -hydride elimination side reaction. Overall, these results provide strong evidence for the involvement of high-valent organometallic Ni species, possibly both Ni<sup>III</sup> and Ni<sup>IV</sup> species, in oxidatively induced C–heteroatom bond formation reactions.

Hydroxylation and alkoxylation of arenes are important chemical transformations, as phenols, hydroxylated heteroarenes, and aryl ethers appear in many natural products, pharmaceuticals, and materials,<sup>1</sup> yet traditional phenol synthesis generally exhibits limited substrate scope and may require harsh reaction conditions.<sup>2</sup> Along with the Cu-catalyzed hydroxylation of aryl bromides and iodides,<sup>3</sup> the Pd-catalyzed Buchwald–Hartwig coupling reaction provides a direct and convenient method to form new C<sub>aryl</sub>–O bonds.<sup>4</sup> However, aryl alkoxylation, especially methoxylation, is still challenging due to a slow reductive elimination step or unwanted  $\beta$ -hydride elimination side reactions.<sup>5</sup> By comparison, the Ni-promoted aryl hydroxylation/alkoxylation is less developed,<sup>6</sup> although it is expected that Ni intermediates, including high-valent species, undergo rapid reductive elimination and possibly exhibit limited  $\beta$ -hydride elimination.<sup>7</sup> In addition, the synthesis of phenols via Ni-catalyzed hydrogenolysis of aryl ethers was also reported recently.<sup>8</sup>

More than three decades ago, van Koten et al. have shown that the pincer NCN<sup>−</sup> ligand can support organometallic Ni<sup>III</sup> complexes that are surprisingly stable,<sup>9</sup> as reported also later for a related pincer system.<sup>10</sup> Moreover, Hillhouse et al.<sup>11</sup> and recently Zargarian et al.<sup>12</sup> have reported oxidatively induced reductive elimination of ethers from metallacyclic Ni(alkoxo)–(alkyl) and Ni(alkoxo)(aryl) complexes, respectively, however no high-valent Ni species were detected in these cases. Recently,

our group has employed the tetradentate ligand *N,N'*-di-*tert*-butyl-2,11-diaza[3.3](2,6)-pyridinophane (<sup>t</sup>Bu<sub>4</sub>N4) to isolate organometallic Ni<sup>III</sup> complexes that undergo C–halide and C–C bond formation reactions and are active catalysts for Kumada and Negishi coupling reactions.<sup>13</sup> In order to expand the reactivity of such organometallic Ni<sup>III</sup> centers, we decided to combine the features of the NCN<sup>−</sup> and <sup>t</sup>Bu<sub>4</sub>N4 ligands by developing a hybrid <sup>t</sup>Bu<sub>3</sub>N3C<sup>−</sup> ligand (Scheme 1). Reported

## Scheme 1. Synthesis of Ni<sup>II</sup> and Ni<sup>III</sup> Complexes 1–4



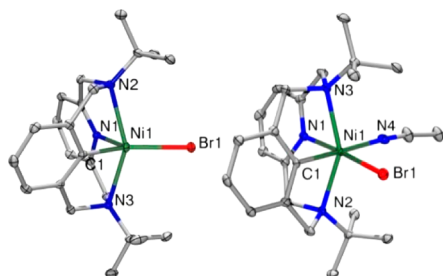
herein is the synthesis, characterization, and reactivity of a series of (<sup>t</sup>Bu<sub>3</sub>N3C)Ni<sup>III</sup> complexes, including a RT stable dicationic [(<sup>t</sup>Bu<sub>3</sub>N3C)Ni<sup>III</sup>(MeCN)<sub>2</sub>]<sup>2+</sup> complex that offers a unique opportunity to study its C–O bond formation reactivity. Importantly, the observed aryl methoxylation and hydroxylation reactions are facilitated by addition of oxidant, suggesting the involvement of Ni<sup>IV</sup> intermediates. Additional studies suggest the Ni<sup>III</sup> species exhibit reduced  $\beta$ -hydride elimination reactivity compared to the Ni<sup>II</sup> analogs, suggesting that high-valent Ni complexes could be employed in a range of oxidatively induced C–heteroatom bond formation reactions.

The Ni<sup>II</sup> precursor (<sup>t</sup>Bu<sub>3</sub>N3C)Ni<sup>II</sup>Br (**1**) was prepared by the oxidative addition of <sup>t</sup>Bu<sub>3</sub>N3CBr to Ni(COD)<sub>2</sub> in THF at RT (Scheme 1).<sup>14</sup> Complex **1** is paramagnetic with an effective

Received: April 20, 2015

Published: June 8, 2015

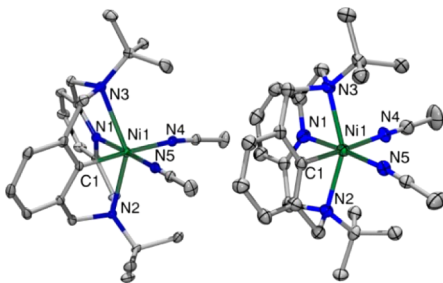
magnetic moment  $\mu_{\text{eff}}$  of  $2.94 \mu_{\text{B}}$  as determined by the Evans method, suggesting an  $S = 1$  ground state. The single crystal X-ray structure of **1** reveals the  ${}^t\text{BuN3C}^-$  ligand acts as a tetradentate ligand, which along with one bromide ligand creates an uncommon trigonal bipyramidal  $\text{Ni}^{\text{II}}$  complex (Figure 1, left).



**Figure 1.** ORTEP representation (50% probability thermal ellipsoids) of **1** (left) and the cation of **2** (right). Selected bond distances (Å): **1**: Ni1–C1, 1.9181(3); Ni1–N1, 1.9660(3); Ni1–N2, 2.3986(3); Ni1–N3, 2.3734(2); Ni1–Br1, 2.4068(2); **2**: Ni1–C1, 1.8872(1); Ni1–N1, 1.9478(1); Ni1–N2, 2.3121(1); Ni1–N3, 2.2913(1); Ni1–Br1, 2.3895(1); Ni1–N4, 2.0089(1).

The Ni1–C1 bond distance of 1.918 Å is shorter than the Ni1–N1 bond distance of 1.966 Å, as expected for the stronger  $\sigma$  donor organic ligand, while the axial Ni– $\text{N}_{\text{amine}}$  distances are longer at  $\sim 2.38$  Å. Interestingly, the cyclic voltammetry (CV) of **1** in 0.1 M  $\text{Bu}_4\text{NBF}_4/\text{THF}$  reveals an accessible oxidation potential at  $-0.61$  V vs  $\text{Fc}^+/\text{Fc}$  (Figure S33) that is tentatively assigned to the  $\text{Ni}^{\text{II/III}}$  redox couple. Indeed, **1** can be readily oxidized with various oxidants ( $\text{CuBr}_2$ ,  $\text{NOBF}_4$ , and  $\text{FcPF}_6$ ) in MeCN at RT to yield stable green products  $[({}^t\text{BuN3C})\text{Ni}^{\text{III}}\text{Br}(\text{MeCN})]\text{X}$  ( $\text{X} = \text{Br}$ ,  $\text{BF}_4$ , or  $\text{PF}_6$ , Scheme 1). The single crystal X-ray structure of  $[({}^t\text{BuN3C})\text{Ni}^{\text{III}}\text{Br}(\text{MeCN})]\text{PF}_6$ , **2**, reveals the  $\text{Ni}^{\text{III}}$  center adopts a distorted octahedral geometry – as expected for a  $d^7$  ion, with the amine donors in the axial positions. The Ni–ligand bond distances in **2** are all shorter than those in **1**, further supporting the formation of a  $\text{Ni}^{\text{III}}$  center (Figure 1).<sup>9,13</sup> Finally, the CV of **2** in 0.1 M  $\text{Bu}_4\text{NBF}_4/\text{MeCN}$  reveals a reversible  $\text{Ni}^{\text{III/II}}$  reduction wave at  $-0.59$  V vs  $\text{Fc}^+/\text{Fc}$  (Figure S35),<sup>14</sup> similar to that observed for **1**.

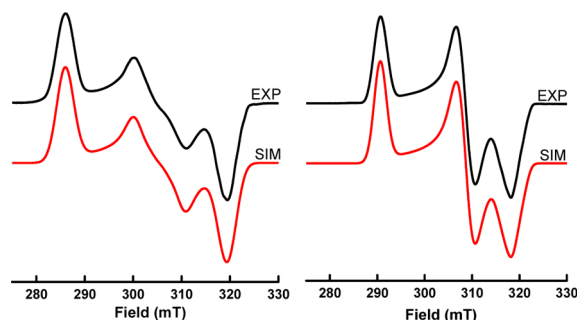
When **1** is treated with 1 equiv of  $\text{TiPF}_6$ , the diamagnetic complex  $[({}^t\text{BuN3C})\text{Ni}^{\text{II}}(\text{MeCN})_2]\text{PF}_6$  (**3**) could be generated (Scheme 1). The solid state structure of **3** reveals the  $\text{Ni}^{\text{II}}$  center adopts a pseudosquare planar geometry (Figure 2, left), in which the two axial Namine donors coordinate very weakly and that



**Figure 2.** ORTEP representation (50% probability thermal ellipsoids) of the cations of **3** (left) and **4** (right). Selected bond distances (Å): **3**: Ni1–C1, 1.8819(1); Ni1–N1, 1.9152(1); Ni1–N2, 2.5527(1); Ni1–N3, 2.5245(1); Ni1–N4, 1.9413(1); Ni1–N5, 1.8973(1); **4**: Ni1–C1, 1.9018(1); Ni1–N1, 1.9287(1); Ni1–N2, 2.2727(1); Ni1–N3, 2.2593(1); Ni1–N4, 2.0045(1); Ni1–N5, 1.9801(1).

may explain why **3** is diamagnetic. However, since the axial amine donors of  ${}^t\text{BuN3C}^-$  in **3** are optimally positioned to stabilize an octahedral geometry, it is expected that **3** can be easily oxidized despite being a monocationic species. Indeed, its CV in 0.1 M  $\text{Bu}_4\text{NBF}_4/\text{MeCN}$  reveals an oxidation potential at  $-0.61$  V vs  $\text{Fc}^+/\text{Fc}$  that is also assigned to the  $\text{Ni}^{\text{II/III}}$  redox couple (Figure S36).<sup>15</sup> Accordingly, **3** can be oxidized with 1 equiv of  $\text{NOBF}_4$ ,  $\text{FcPF}_6$ , or  $\text{AgSbF}_6$  to generate air-stable green complexes  $[({}^t\text{BuN3C})\text{Ni}^{\text{III}}(\text{MeCN})_2]\text{X}_2$  ( $4\text{X}_2$ ,  $\text{X} = \text{BF}_4$ ,  $\text{SbF}_6$ , or  $\text{PF}_6$ , Scheme 1).<sup>14</sup> The solid-state structure of  $[({}^t\text{BuN3C})\text{Ni}^{\text{III}}(\text{MeCN})_2](\text{PF}_6)(\text{SbF}_6)$  reveals the equatorial Ni–ligand bond distances in **4** are slightly longer than those in **3**, while the axial Ni–Namine bond distances are significantly shorter than those in **3**, as expected for a change in the Ni coordination geometry from pseudosquare planar to distorted octahedral (Figure 2, right).

The  $\text{Ni}^{\text{III}}$  complexes **2** and **4** are paramagnetic and exhibit effective magnetic moments  $\mu_{\text{eff}}$  of 1.68 and  $1.71 \mu_{\text{B}}$  at 298 K, corresponding to one unpaired electron. Their EPR spectra (77 K, PrCN glass) reveal rhombic signals with  $g_{\text{ave}}$  values of 2.145 for **2** and 2.127 for **4**, along with superhyperfine coupling to the two axial N donors ( $I = 1$ ) observed in the  $g_z$  direction (Figure 3). In

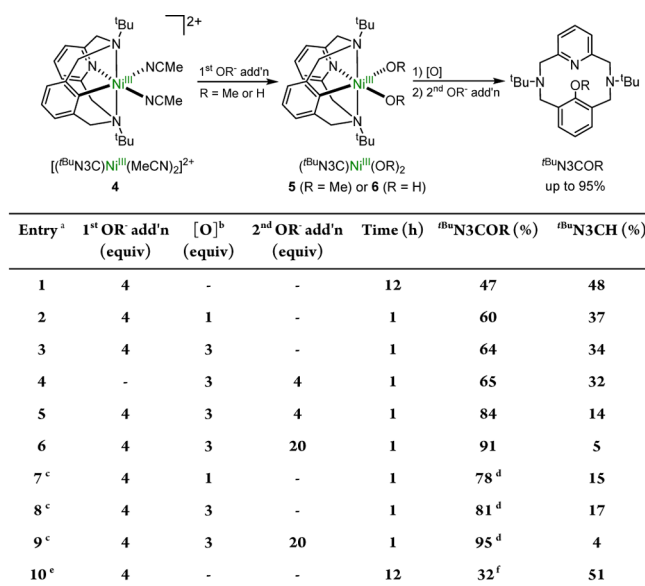


**Figure 3.** Experimental (PrCN, 77 K) and simulated EPR spectra of **2** (left) and **4** (right). The following parameters were used for simulations: **2**,  $g_x = 2.272$ ;  $g_y = 2.128$  ( $A_{\text{Br}} = 26.5$  G);  $g_z = 2.035$  ( $A_{2\text{N}} = 10.0$  G,  $A_{\text{Br}} = 5.0$  G); **4**,  $g_x = 2.236$ ;  $g_y = 2.105$ ;  $g_z = 2.041$  ( $A_{2\text{N}} = 13.5$  G).

addition, superhyperfine coupling to the Br atom ( $I = 3/2$ ) is observed for **2** along the  $g_y$  and  $g_z$  directions. Taken together, the observed structural and EPR parameters for complexes **2** and **4** strongly suggest the presence of a distorted octahedral  $\text{Ni}^{\text{III}}$   $d^7$  center with a  $d_{z^2}$  ground state.<sup>9,13</sup>

Since the  ${}^t\text{BuN3C}^-$  ligand can stabilize a  $\text{Ni}^{\text{III}}$  center with two *cis* coordination sites available for exogenous ligands, we employed **4** to study C-heteroatom bond formation reactions from high-valent Ni complexes. When **4** was reacted with 4 equiv NaOMe in MeCN/MeOH, the red complex  $({}^t\text{BuN3C})\text{Ni}^{\text{III}}(\text{OMe})_2$ , **5**, was obtained (Scheme 2). The identity of **5** was confirmed by a low-resolution X-ray crystal structure that confirms the atom connectivity, the conformation of the  ${}^t\text{BuN3C}^-$  ligand, and the distorted octahedral geometry of the  $\text{Ni}^{\text{III}}$  center (Figure S4).<sup>14</sup> Its EPR spectrum reveals a rhombic signal and  $g_{\text{ave}} = 2.192$ , along with superhyperfine coupling to the two axial N donors ( $I = 1$ ) observed in the  $g_z$  direction (Figure S5). The coordination environment of the Ni center in **5** is also supported by the ordering of the  $g_{\text{ave}}$  values:  $2.192$  for **5** >  $2.145$  for **2** >  $2.127$  for **4**, as expected when replacing weakly back-bonding MeCN ligands with stronger  $\sigma$ -donor and  $\pi$ -donor bromide or methoxide ligands.

Complex **5** decomposes at RT in THF overnight, and analysis of the reaction mixture by ESI-MS and NMR reveals two major

Scheme 2. Formation and C–O Bond Formation Reactivity of Complexes 5 and 6 under Various Conditions<sup>a</sup>

<sup>a</sup>(a) For entries 1–6, the reactions were performed in THF/MeOH, and NaOMe was used as methoxide source; the yields were determined by GC-MS (ref 12). (b) [O] is PhI(PyOMe)<sub>2</sub>OTf<sub>2</sub>. (c) Reactions were performed in THF/CD<sub>3</sub>OD, and KOCD<sub>3</sub> was used as methoxide source. (d) The product is <sup>t</sup>Bu<sub>3</sub>N<sub>3</sub>COCD<sub>3</sub>. (e) The reaction was performed in THF/H<sub>2</sub>O, and LiOH was used as OH<sup>-</sup> source. (f) The product is <sup>t</sup>Bu<sub>3</sub>N<sub>3</sub>COH.

products, <sup>t</sup>Bu<sub>3</sub>N<sub>3</sub>COMe (47% yield) and <sup>t</sup>Bu<sub>3</sub>N<sub>3</sub>CH (48% yield) in a ~1:1 ratio (Scheme 2, entry 1). Interestingly, when NaOCD<sub>3</sub> in CD<sub>3</sub>OH was used to generate *d*<sub>6</sub>-5, <sup>t</sup>Bu<sub>3</sub>N<sub>3</sub>CD, not <sup>t</sup>Bu<sub>3</sub>N<sub>3</sub>CH, was observed by GC-MS, suggesting that its formation involves β-hydride elimination from a (<sup>t</sup>Bu<sub>3</sub>N<sub>3</sub>C)Ni(OMe) intermediate.<sup>14</sup> Moreover, the addition of 2 equiv of NaOMe to 3 results in rapid formation of <sup>t</sup>Bu<sub>3</sub>N<sub>3</sub>CH in 99% yield, suggesting that a Ni<sup>II</sup> species (<sup>t</sup>Bu<sub>3</sub>N<sub>3</sub>C)Ni<sup>II</sup>(OMe) is more prone to β-hydride elimination.<sup>8b</sup> Therefore, the addition of an appropriate oxidant may limit the formation of such Ni<sup>II</sup> species and the β-hydride elimination side reaction. Indeed, the addition of PhI(PyOMe)<sub>2</sub>OTf<sub>2</sub>, an oxidant used recently by Ritter et al. in Ni-mediated C–F bond formation,<sup>16</sup> improved the yield of <sup>t</sup>Bu<sub>3</sub>N<sub>3</sub>COMe to 60% and 64% when 1 or 3 equiv of oxidant was added, respectively (Scheme 2, entries 2 and 4). While the order of oxidant and OMe<sup>-</sup> addition does not affect the product yields (Scheme 2, entries 3 and 4), the addition of excess OMe<sup>-</sup> (4 or 20 equiv) in the presence of 3 equiv of oxidant increases the <sup>t</sup>Bu<sub>3</sub>N<sub>3</sub>COMe yield to 84% and 91% (Scheme 2, entries 5 and 6).<sup>17</sup> In addition, presence of both excess oxidant and methoxide dramatically reduces the extent of β-hydride elimination down to 5% <sup>t</sup>Bu<sub>3</sub>N<sub>3</sub>CH. Since D atoms are expected to undergo β-hydride elimination slower than H atoms,<sup>8b,18</sup> the oxidation of *in situ* generated (<sup>t</sup>Bu<sub>3</sub>N<sub>3</sub>C)Ni<sup>III</sup>(OCD<sub>3</sub>)<sub>2</sub> with 1 equiv of oxidant led to <sup>t</sup>Bu<sub>3</sub>N<sub>3</sub>COCD<sub>3</sub> in 78% yield (Scheme 2, entry 7), while addition of excess OCD<sub>3</sub><sup>-</sup> (20 equiv) and 3 equiv of oxidant generated <sup>t</sup>Bu<sub>3</sub>N<sub>3</sub>COCD<sub>3</sub> in an excellent 95% yield (Scheme 2, entry 9). Overall, these results strongly suggest that high-valent Ni<sup>III</sup> species exhibit limited β-hydride elimination vs the Ni<sup>II</sup> analogs and are also capable of efficient oxidatively induced C–O bond formation reactivity, thus making them viable reactive inter-

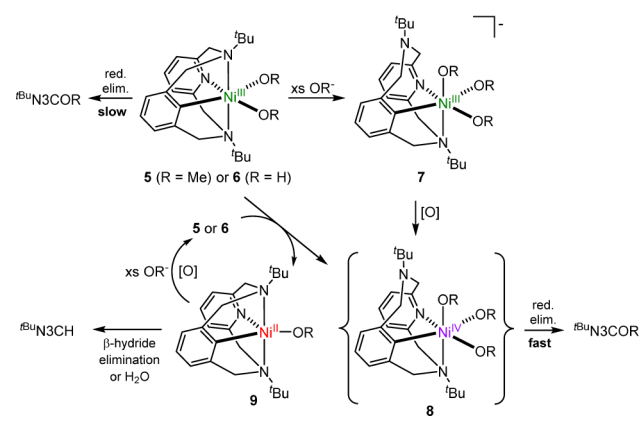
mediates in Ni-catalyzed C-heteroatom bond formation reactions.

In addition to aryl methoxylation, the hydroxylation of the <sup>t</sup>Bu<sub>3</sub>N<sub>3</sub>C<sup>-</sup> ligand was also investigated. When 4 was reacted with 4 equiv of LiOH in THF/H<sub>2</sub>O, a red complex assigned as (<sup>t</sup>Bu<sub>3</sub>N<sub>3</sub>C)Ni<sup>III</sup>(OH)<sub>2</sub>, 6, was prepared *in situ* (Scheme 2). Its EPR spectrum reveals a rhombic signal and *g*<sub>ave</sub> = 2.186, along with superhyperfine coupling to the two axial N donors (*I* = 1) observed in the *g*<sub>z</sub> direction (Figure S6), which is similar to the EPR spectrum of 5.<sup>14</sup> Complex 6 decomposes at RT to generate two major products, <sup>t</sup>Bu<sub>3</sub>N<sub>3</sub>COH and <sup>t</sup>Bu<sub>3</sub>N<sub>3</sub>CH, in 32% and 51% yields, respectively (Scheme 2, entry 10). The increased yield of <sup>t</sup>Bu<sub>3</sub>N<sub>3</sub>CH vs <sup>t</sup>Bu<sub>3</sub>N<sub>3</sub>COH is likely due to ligand protonation in the presence of water, as shown independently for 1 that generates <sup>t</sup>Bu<sub>3</sub>N<sub>3</sub>CH in the presence of H<sub>2</sub>O. While we could not improve the <sup>t</sup>Bu<sub>3</sub>N<sub>3</sub>COH yield due to the limited solubility of the oxidant in THF/H<sub>2</sub>O, these results suggest aryl hydroxylation can also occur from a Ni<sup>III</sup> center. Interestingly, when the reaction of 4 with excess LiOH was monitored by EPR, a new transient signal (*g*<sub>⊥</sub> = 2.094, *g*<sub>||</sub> = 2.005) was observed upon decomposition of 6 that reaches its maximum intensity in ~70 min and then disappears in ~3 h.<sup>14</sup> This inverted axial EPR spectrum suggests a Ni<sup>III</sup> species with a *d*<sub>x<sup>2</sup>-y<sup>2</sup> ground state,<sup>9b,c,19</sup> and we tentatively propose the formation of a five-coordinate Ni<sup>III</sup> species with trigonal symmetry or an intermediate with a third OH<sup>-</sup> coordinated to the Ni<sup>III</sup> center (see below).</sub>

Given that the C–O bond formation reactivity of the Ni<sup>III</sup> complex 5 is favored by addition of the PhI(PyOMe)<sub>2</sub>OTf<sub>2</sub> oxidant, the possible formation of a Ni<sup>IV</sup> intermediate can be invoked. Recently, Sanford et al. have elegantly shown the isolation of organometallic Ni<sup>IV</sup> complexes that undergo various C–C and C-heteroatom reductive elimination reactions.<sup>7c</sup> In our case, the CV of 5 in MeCN reveals an irreversible oxidation wave at 0.55 V vs Fc<sup>+</sup>/Fc, which is tentatively assigned to the Ni<sup>III/IV</sup> redox couple (Figure S38). While this oxidation potential should be easily accessed by PhI(PyOMe)<sub>2</sub>(OTf)<sub>2</sub>,<sup>16</sup> no Ni<sup>IV</sup> species was observed when 5 (or 6) was reacted with PhI(PyOMe)<sub>2</sub>OTf<sub>2</sub>, suggesting that the corresponding Ni<sup>IV</sup> species is too unstable to be observed and rapidly undergoes reductive elimination. By comparison, when 3 was reacted with PhI(PyOMe)<sub>2</sub>OTf<sub>2</sub>, only the corresponding Ni<sup>III</sup> species 4 was observed, while the reaction of isolated 4 with 1 equiv of PhI(PyOMe)<sub>2</sub>OTf<sub>2</sub> leads to no further oxidation. Importantly, the addition to 5 of milder oxidants such as Fc<sup>+</sup> did not increase the reaction rate or the yield of <sup>t</sup>Bu<sub>3</sub>N<sub>3</sub>COMe, suggesting that the role of the PhI(PyOMe)<sub>2</sub>OTf<sub>2</sub> oxidant is not merely to circumvent the reduction of the Ni<sup>III</sup> center.<sup>14</sup>

Based on the results above, a mechanism involving Ni<sup>III</sup> disproportionation and a possible Ni<sup>IV</sup> intermediate<sup>7c</sup> is proposed (Scheme 3). Since the presence of excess OMe<sup>-</sup> improves the yield of <sup>t</sup>Bu<sub>3</sub>N<sub>3</sub>COMe, an intermediate 7 with a third OR<sup>-</sup> coordinated to the Ni<sup>III</sup> center may form, corresponding to the transient EPR signal observed during the decomposition of 6. Such a tris-alkoxide Ni<sup>III</sup> intermediate could be easily oxidized by PhI(PyOMe)<sub>2</sub>OTf<sub>2</sub> to generate the Ni<sup>IV</sup> intermediate 8 that is expected to undergo rapid C–O reductive elimination to generate <sup>t</sup>Bu<sub>3</sub>N<sub>3</sub>COR. In the absence of the oxidant, either a slow C–O reductive elimination may occur from the Ni<sup>III</sup> center, similar to the proposed C–C bond formation in Ni-catalyzed cross-coupling reactions,<sup>20</sup> or two molecules of (<sup>t</sup>Bu<sub>3</sub>N<sub>3</sub>C)Ni<sup>III</sup>(OR)<sub>2</sub> (i.e., 5 or 6) could undergo a slow disproportionation reaction along with OR<sup>-</sup> group transfer to

Scheme 3. Proposed Mechanisms Leading to Oxidatively Induced C–O Bond formation



generate intermediate **8** and **9**, which will ultimately generate  $t\text{BuN}_3\text{COR}$  and  $t\text{BuN}_3\text{CH}$  in a  $\sim 1:1$  ratio, as observed experimentally (Scheme 2). The presence of excess oxidant and  $\text{OR}^-$  can also promote a rapid oxidation of **9** to generate **5/6** and thus suppress the formation of the  $t\text{BuN}_3\text{CH}$  side product. Overall, since only a strong oxidant, not  $\text{Fc}^+$ , increases the reaction rate and  $t\text{BuN}_3\text{COMe}$  yield from **5**, a mechanism involving a transient  $\text{Ni}^{\text{IV}}$  intermediate is more likely.

In conclusion, the use of a newly developed tetradentate pyridinophane  $t\text{BuN}_3\text{C}^-$  ligand has allowed the isolation and characterization of several organometallic  $\text{Ni}^{\text{III}}$  complexes. In particular, the  $[(t\text{BuN}_3\text{C})\text{Ni}^{\text{III}}(\text{MeCN})_2]^{2+}$  disolvento complex with two available *cis* coordination sites enabled the generation of organometallic  $\text{Ni}^{\text{III}}$ -dimethoxide and  $\text{Ni}^{\text{III}}$ -dihydroxide species that were shown to undergo aryl methoxylation and hydroxylation, respectively. Importantly, this C–O bond formation reactivity is promoted by addition of an oxidant, which also limits the  $\beta$ -hydride elimination side reaction. Overall, these results suggest that high-valent Ni complexes are viable intermediates in Ni-catalyzed aryl hydroxylation and methoxylation reactions. Future research efforts are aimed toward the development of catalytic applications for these high-valent organometallic Ni species and possibly the detection and isolation of  $\text{Ni}^{\text{IV}}$  intermediates.

## ■ ASSOCIATED CONTENT

### Supporting Information

Synthetic details, spectroscopic characterization, reactivity studies, and crystallographic data. The Supporting Information is available free of charge on the ACS Publications website at DOI: 10.1021/jacs.5b04082.

## ■ AUTHOR INFORMATION

### Corresponding Author

\*mirica@wustl.edu

### Notes

The authors declare no competing financial interest.

## ■ ACKNOWLEDGMENTS

We thank National Science Foundation (CHE1255424) for support.

## ■ REFERENCES

- (1) (a) Tyman, J. H. P. *Synthetic and Natural Phenols*; Elsevier: Amsterdam, The Netherlands, 1996. (b) Elias, H.-G. *An Introduction to Polymer Science*; Wiley-VCH: Weinheim, Germany, 1997.
- (2) Smith, M. B.; March, J. *March's Advanced Organic Chemistry*; 6th ed.; John Wiley & Sons, Inc.: Hoboken, NJ, 2007.
- (3) (a) Alonso, D. A.; Najera, C.; Pastor, I. M.; Yus, M. *Chem.—Eur. J.* **2010**, *16*, 5274. (b) Tlili, A.; Xia, N.; Monnier, F.; Taillefer, M. *Angew. Chem., Int. Ed.* **2009**, *48*, 8725.
- (4) (a) Widenhoefer, R. A.; Zhong, H. A.; Buchwald, S. L. *J. Am. Chem. Soc.* **1997**, *119*, 6787. (b) Mann, G.; Incarvito, C.; Rheingold, A. L.; Hartwig, J. F. *J. Am. Chem. Soc.* **1999**, *121*, 3224. (c) Muci, A. R.; Buchwald, S. L. *Top. Curr. Chem.* **2002**, *219*, 131. (d) Enthaler, S.; Company, A. *Chem. Soc. Rev.* **2011**, *40*, 4912.
- (5) (a) Vorogushin, A. V.; Huang, X. H.; Buchwald, S. L. *J. Am. Chem. Soc.* **2005**, *127*, 8146. (b) Gowrisankar, S.; Neumann, H.; Beller, M. *Chem.—Eur. J.* **2012**, *18*, 2498.
- (6) (a) Mann, G.; Hartwig, J. F. *J. Org. Chem.* **1997**, *62*, 5413. (b) Honda, K.; Cho, J.; Matsumoto, T.; Roh, J.; Furutachi, H.; Toshi, T.; Kubo, M.; Fujinami, S.; Ogura, T.; Kitagawa, T.; Suzuki, M. *Angew. Chem., Int. Ed.* **2009**, *48*, 3304.
- (7) (a) Zuo, Z. W.; Ahneman, D. T.; Chu, L. L.; Terrett, J. A.; Doyle, A. G.; MacMillan, D. W. C. *Science* **2014**, *345*, 437. (b) Tellis, J. C.; Primer, D. N.; Molander, G. A. *Science* **2014**, *345*, 433. (c) Camasso, N. M.; Sanford, M. S. *Science* **2015**, *347*, 1218.
- (8) (a) Sergeev, A. G.; Hartwig, J. F. *Science* **2011**, *332*, 439. (b) Kelley, P.; Lin, S. B.; Edouard, G.; Day, M. W.; Agapie, T. *J. Am. Chem. Soc.* **2012**, *134*, 5480.
- (9) (a) Grove, D. M.; van Koten, G.; Zoet, R.; Murrall, N. W.; Welch, A. J. *J. Am. Chem. Soc.* **1983**, *105*, 1379. (b) Grove, D. M.; Van Koten, G.; Mul, P.; Van der Zeijden, A. A. H.; Terheijden, J.; Zoutberg, M. C.; Stam, C. H. *Organometallics* **1986**, *5*, 322. (c) van de Kuil, L. A.; Veldhuizen, Y. S. J.; Grove, D. M.; Zwikker, J. W.; Jennekens, L. W.; Drenth, W.; Smeets, W. J. J.; Spek, A. L.; van Koten, G. *J. Organomet. Chem.* **1995**, *488*, 191. (d) Grove, D. M.; van Koten, G.; Mul, P.; Zoet, R.; van der Linden, J. G. M.; Legters, J.; Schmitz, J. E. J.; Murrall, N. W.; Welch, A. J. *Inorg. Chem.* **1988**, *27*, 2466.
- (10) Spasyuk, D. M.; Zargarian, D.; van der Est, A. *Organometallics* **2009**, *28*, 6531.
- (11) (a) Matsunaga, P. T.; Hillhouse, G. L.; Rheingold, A. L. *J. Am. Chem. Soc.* **1993**, *115*, 2075. (b) Matsunaga, P. T.; Mavropoulos, J. C.; Hillhouse, G. L. *Polyhedron* **1995**, *14*, 175. (c) Koo, K. M.; Hillhouse, G. L.; Rheingold, A. L. *Organometallics* **1995**, *14*, 456. (d) Han, R. Y.; Hillhouse, G. L. *J. Am. Chem. Soc.* **1997**, *119*, 8135.
- (12) Cloutier, J. P.; Vabre, B.; Mounang-Soume, B.; Zargarian, D. *Organometallics* **2015**, *34*, 133.
- (13) Zheng, B.; Tang, F.; Luo, J.; Schultz, J. W.; Rath, N. P.; Mirica, L. M. *J. Am. Chem. Soc.* **2014**, *136*, 6499.
- (14) See Supporting Information.
- (15) The CV of **1** in MeCN shows a more reversible redox behavior similar to **3**, indicating that MeCN likely coordinates to the Ni center and possibly replaces the bromide ligand in solution (Figure S33). In addition, the NMR of **1** in MeCN reveals the presence of a diamagnetic species, further suggesting solvent coordination to the Ni center (Figure S3).
- (16) (a) Weiss, R.; Seubert, J. *Angew. Chem., Int. Ed.* **1994**, *33*, 891. (b) Lee, E.; Hooker, J. M.; Ritter, T. *J. Am. Chem. Soc.* **2012**, *134*, 17456.
- (17) Addition of radical traps such as DMPO and TEMPO did not affect the  $t\text{BuN}_3\text{COMe}$  yield, suggesting that a radical mechanism is unlikely.
- (18) Gomez-Gallego, M.; Sierra, M. A. *Chem. Rev.* **2011**, *111*, 4857.
- (19) Iluc, V. M.; Miller, A. J. M.; Anderson, J. S.; Monreal, M. J.; Mehn, M. P.; Hillhouse, G. L. *J. Am. Chem. Soc.* **2011**, *133*, 13055.
- (20) (a) Breitenfeld, J.; Ruiz, J.; Wodrich, M. D.; Hu, X. *J. Am. Chem. Soc.* **2013**, *135*, 12004. (b) Breitenfeld, J.; Wodrich, M. D.; Hu, X. *Organometallics* **2014**, *33*, 5708.